

Facile preparation of antifouling nanofiltration membrane by grafting zwitterions for reuse of shale gas wastewater

Original

Facile preparation of antifouling nanofiltration membrane by grafting zwitterions for reuse of shale gas wastewater / Hu, Minli; Wu, Qidong; Chen, Chen; Liang, Songmiao; Liu, Yuanhui; Bai, Yuhua; Tiraferri, Alberto; Liu, Baicang. - In: SEPARATION AND PURIFICATION TECHNOLOGY. - ISSN 1383-5866. - 276:(2021), p. 119310. [10.1016/j.seppur.2021.119310]

Availability:

This version is available at: 11583/2915974 since: 2021-07-30T11:11:38Z

Publisher:

Elsevier B.V.

Published

DOI:10.1016/j.seppur.2021.119310

Terms of use:

This article is made available under terms and conditions as specified in the corresponding bibliographic description in the repository

Publisher copyright

(Article begins on next page)

1 Facile preparation of antifouling nanofiltration
2 membrane by grafting zwitterions for reuse of
3 shale gas wastewater

4 *Minli Hu^{a,b}, Qidong Wu^{a,b}, Chen Chen^c, Songmiao Liang^d, Yuanhui Liu^{a,b}, Yuhua Bai^e,*

5 *Alberto Tiraferri^f, Baicang Liu^{a,b,*}*

6 ^aKey Laboratory of Deep Earth Science and Engineering (Ministry of Education), College of
7 Architecture and Environment, Institute of New Energy and Low-Carbon Technology,
8 Institute for Disaster Management and Reconstruction, Sichuan University, Chengdu, Sichuan
9 610207, PR China

10 ^bYibin Institute of Industrial Technology, Sichuan University Yibin Park, Section 2, Lingang
11 Ave, Cuiping District, Yibin, Sichuan 644000, PR China

12 ^cLitree Purifying Technology Co., Ltd, Haikou, Hainan 571126, PR China

13 ^dVontron Technology Co., Ltd, Guiyang 550018, PR China

14 ^eInfrastructure Construction Department, Chengdu University, Chengdu 610106, PR China

15 ^fDepartment of Environment, Land and Infrastructure Engineering, Politecnico di Torino,
16 Corso Duca degli Abruzzi 24, 10129 Turin, Italy

17 **Abstract:** Complex organic matter causes severe fouling when membranes are applied for
18 shale gas wastewater (SGW) treatment. This study reports the grafting of a zwitterionic
19 polymer brush consisting of poly (sulfobetaine methacrylate) (PSBMA) onto the surface of a
20 commercial nanofiltration (NF) membrane via electron transfer-atom transfer radical
21 polymerization (ARGET-ATRP) to achieve anti-fouling property, especially against organic
22 foulants. Compared to the pristine NF membranes, the PSBMA-grafted NF membrane
23 showed high performance when challenged by SGW as a feed stream: (1) The productivity
24 was significantly improved during long-term operation, with a 64.28% increase in flux at 50%
25 recovery rate of SGW, while maintaining a near constant ion removal rate; (2) According to
26 fluorescence regional integration under the Excitation—Emission—Matrix Spectra, the
27 removal of protein-like organic matters and humus-like organic matters increased by 34.01%
28 and 16.48%, respectively; (3) The XDLVO theory demonstrated that the hydrophobic
29 interactions between the membrane surface and organic foulants were reduced by increasing
30 the Lewis acid-base interaction energy. The proposed anti-fouling zwitterionic membranes
31 has potential in industrial application for the on-site reuse of SGW.

32 **Keywords:** Shale gas wastewater (SGW); Membrane fouling; Surface modification; Poly
33 (sulfobetaine methacrylate) (PSBMA); Nanofiltration (NF)

34

35 1. Introduction

36 The “shale gas revolution” was first successfully practiced in the USA to ensure energy
37 security. China is currently accelerating the pace of shale gas exploration and development [1,
38 2]. According to evaluations made by the Chinese government, China has $25.08 \times 10^{12} \text{ m}^3$ of
39 technically recoverable shale gas reserves, positioning it as one of the most promising
40 countries in the world for shale gas development [3, 4]. However, the shale gas exploration
41 process consumes large amounts of freshwater resources and generates vast quantities of shale
42 gas wastewater (SGW) [5, 6]. In the Sichuan Basin, China, the average freshwater demand of
43 a shale gas well is 23,650–34,000 m^3 , and 8-70% of the shale gas flowback and produced
44 water is returned to the ground [7-9].

45 SGW in the Sichuan Basin contains low to moderate salinity (total dissolved solids < 30
46 g/L), complex and heterogeneous organic compounds, and its treatment to safe standard is
47 costly and challenging [10]. Currently, most SGW both in China and USA are reused for
48 fracturing in new wells, since the recycling of the fracturing fluid can achieve both cost
49 savings and environmental pollution reduction [11-13]. The effective removal of divalent ions
50 is critical for SGW reuse to avoid scaling on production equipment and in the shale formation
51 [14-16]. Based on the salinity and composition of the Sichuan Basin SGW, nanofiltration (NF)
52 membrane technology is a suitable and promising candidate for purification with the aim to
53 remove divalent ions and maintain a stable production of shale gas [9, 17, 18]. However,
54 membrane fouling is a major drawback that restricts the application of NF membranes and
55 can lead to increased energy consumption, alongside increased frequency of chemical
56 cleaning and shortened membrane life [19-21]. In general, membrane fouling is the result of a
57 complex series of physicochemical interactions between the membrane surface and the
58 fouling agents [21, 22][23, 24]. The complex organic mixture in SGW is arguably the main
59 cause of NF membrane fouling in this application [25]. Effective pretreatments are often used

60 to improve the NF performance and ensure its sustainable operation [13, 26]. The
61 combination of coagulation [27], adsorption [28], ozone pre-oxidation [29], or biological
62 treatment technology [30] with UF has been applied for pre-treatment. However, NF fouling
63 is still inevitable and few studies have focused on the properties of the NF membrane itself to
64 improve their resistance to contamination from SGW foulants.

65 The synthesis of new antifouling membranes through surface modification is an effective
66 way to control membrane fouling [22], and direct modification of the membrane surface is
67 ideal for large-scale processing applications [31-33]. Antifouling membrane modification
68 materials are mainly polymers, and the introduction of hydrophilic monomers or polar groups
69 can significantly improve the membrane antifouling performance [34, 35]. Commonly used
70 modifiers include: poly(vinyl alcohol) (PVA) [36], polyethylene glycol (PEG) [37], MXene
71 [38], polydopamine (PDA) [39], and polyurethane[40]. Compared to other hydrophilic
72 materials, zwitterionic polymer brushes (e.g., sulfobetaine methacrylate, SBMA) comprising
73 both anionic and cationic end groups exhibit excellent antifouling performance at high salt
74 concentrations [41], because of their overall electrical neutrality and strong hydration ability.
75 SBMA can form a tight hydration layer on the surface of membrane materials, which can
76 weaken the interaction force between organic pollutants and the membrane surface [21, 31,
77 41-48]. In particular, this mechanism is effective against hydrophobic organic substances,
78 such as protein-like and humic-like matter, which accounts for a relatively high proportion of
79 the organics in SGW [28, 29, 35, 49]. Typical modification methods include chemical
80 grafting, physical coating, and polymer modification [44, 45, 47]. Modification through
81 activators regenerated by electron transfer–atom transfer radical polymerization (ARGET-
82 ATRP) is suitable to modify the membrane surface at large scale under routine industrial
83 conditions in an easy and quick way, because it only require a low dosage of copper catalyst
84 and has high tolerance to oxygen presence [50, 51]. Our previous study used ARGET-ATRP

85 method to graft [2-(methacryloyloxy) ethyl] dimethyl(3-sulfopropyl) ammonium hydroxide
86 (DMAPS) on the surface of self-made green ultrafiltration membranes showing highly
87 promising results also for other membrane processes and applications [52].

88 In this work, we tune and apply this procedure to fabricate a high-performance NF
89 membrane deployed to treat SGW with the goal of reuse. The relationship between membrane
90 surface modification and improved antifouling performance is investigated upon grafting a
91 zwitterionic polymer brush PSBMA onto the surface of a commercial NF membranes via an
92 ARGET-ATRP method. The water flux decline rate is analyzed and evaluated in the light of
93 the membrane surface properties and the degree of organic deposition. The effect of
94 membrane fouling is discussed using the XDLVO theory. The purpose of this paper is to
95 provide valuable information on ways to reduce NF membrane fouling by designing NF
96 membranes suitable for shale gas wastewater treatment.

97

98 **2. Materials and methods**

99 2.1. Pretreatment of the raw water

100 The raw water in this study was acquired from one of the reservoirs of the Weiyuan shale
101 gas play, Sichuan, China. The detailed water quality and the optimal pretreatment conditions
102 were comprehensively analyzed in our previous study [13]. In brief, the optimal pretreatment
103 condition for coagulation involved addition of 900 mg/L ferric chloride hexahydrate
104 ($\text{FeCl}_3 \cdot 6\text{H}_2\text{O}$) followed by 30 min settling. The supernatant was then introduced to the tank of
105 a ultrafiltration system comprising a submerged hollow fiber poly (vinylidene fluoride)
106 (PVDF) UF membrane (Litree Purifying Technology Co., Ltd. Haikou, China with nominal
107 molecular weight cut-off 100 kDa under a constant flux of $50 \text{ L m}^{-2}\text{h}^{-1}$).

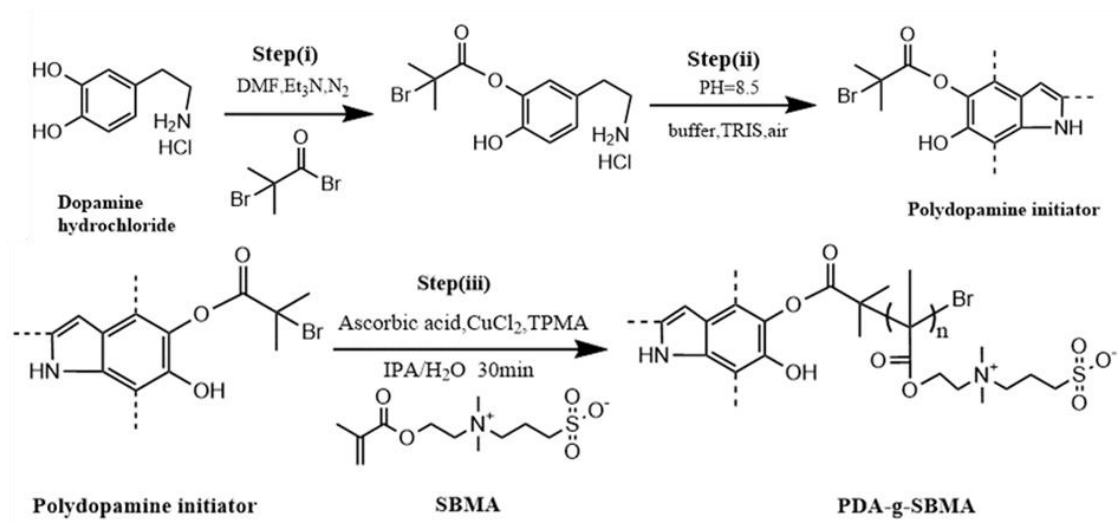
108 2.2. Materials

109 Two types of commercially available NF membranes were employed in this work, namely,
110 the membranes referred to as VNF1 (Vontron Membrane Technology Co., Ltd., Guiyang,
111 China), and NF90 (DuPont, USA). Ultrapure water was supplied by a Ulupure ultrapure water
112 purification system (Chengdu, China) with a resistivity of 18.25 M Ω . Sulfobetaine
113 methacrylate (SBMA), sometimes referred to as 3-dimethyl (methacryloyloxyethyl)
114 ammonium propane sulfonate (DMAPS), N,N-dimethylformamide (DMF), l-ascorbic acid,
115 copper (II) chloride, tris (2-pyridylmethyl) amine (TPMA), magnesium sulfate (MgSO₄,
116 anhydrous, reagent plus, $\geq 99.5\%$), and sodium chloride (NaCl, reagent grade, 99%) were
117 obtained from Sigma Aldrich (USA), Dopamine hydrochloride, α -bromoisobutyryl bromide
118 (BiBB, 98%), isopropyl alcohol (IPA), tris (hydroxymethyl) aminomethane (Tris) ($>99.8\%$),
119 and triethylamine (TEA) ($>99\%$), were purchased from Aladdin (China). Sodium sulfate
120 (Na₂SO₄) (anhydrous, $\geq 99\%$), magnesium chloride (MgCl₂) ($\geq 98\%$), and ethylene glycol
121 (99%) were all analytical reagents (Kelong Chemical, Chengdu, China). Glycerol (99.7%)
122 was purchased from VWR (PA, USA). Diiodomethane (99%) was purchased from Macklin
123 (Shanghai, China).

124 2.3 Surface modification of NF membranes

125 The commercial membrane was subject to surface ARGET-ATRP grafting reaction
126 through a typical three-step strategy. The first step involved the preparation of a BiBB-
127 initiator-dopamine solution; after addition of the Tris buffer into this solution to adjust the pH,
128 the commercial membrane was placed into the buffered solution to form a PDA surface
129 coating (second step); the third step encompassed the grafting of SBMA to the membrane
130 surface through the ARGET-ATRP reaction. The detailed steps can be found in **Text S1 (SI)**.

131



132

133 **Scheme. 1.** Proposed modification of NF membranes and reaction products: Step (i)
 134 involved the reaction of dopamine hydrochloride and 2-bromoisobutyryl bromide; Step (ii) in
 135 which the reaction mixture from Step (i) was added to Tris buffer (pH=8.5) to form a BiBB-
 136 initiator-PDA coating; Step (iii) involved the surface initiated ARGET-ATRP reaction with
 137 SBMA from the BiBB-initiator-PDA coating to produce modified membranes with a surface-
 138 grafted SBMA polymer brush.

139

140 2.4. Membrane Characterization

141 The surface chemical composition of the membranes was analyzed via X-ray photoelectron
 142 spectroscopy (XPS) (Axis Supra, Kratos Analytical Ltd., UK) and with a Fourier transform
 143 infrared (FTIR) spectrometer equipped with a diamond attenuated total reflection (ATR)
 144 attachment (Nicolet is iS20, Thermo Fisher Scientific Inc., USA). The membrane surface
 145 morphology and roughness characteristics were obtained by scanning electron microscopy
 146 (SEM) (Regulus 8230, Hitachi, Japan) and atomic force microscopy (AFM, Dimension Icon,
 147 Bruker, Germany), respectively. The zeta potential was evaluated by a SurPASSTM 3
 148 electrokinetic analyzer (Anton Paar, Austria). The dynamic water contact angles were
 149 determined by a contact angle measurement equipment (KRÜSS GmbH, Germany) at room
 150 temperature. More details can be found in our previous study [53] and in **Text S2 (SI)**.

151 2.5 Separation performance of the NF membranes

152 The NF lab unit was thoroughly cleaned before and after each fouling experiment. Prior to
153 each experiment, the membranes were soaked in ultrapure water at room temperature for 24 h
154 and then compacted with ultrapure water at a pressure of 6.89 bar (100 psi) for at least 30 min.
155 The separation performance of the membranes was evaluated at an applied pressure of 20.7
156 bar (300 psi) in a stainless-steel dead-end membrane module (HP 4750, Sterlitech Corp., Kent,
157 WA), with an effective testing area, A , of 14.6 cm^2 . The separation equipment was operated
158 under constant stirring of 300 rpm to minimize concentration polarization effects. Eq. (1) was
159 employed to determine the flux of pure water:

$$160 \quad J = \frac{V}{A \times \Delta t} \quad (1)$$

161 where V (L) is calculated by dividing the permeate water mass collected in a certain
162 interval (Δt) by the water density.

163 The ion filtration performance of the NF membranes was evaluated using inorganic salts
164 (Na_2SO_4 , MgSO_4 , MgCl_2 , NaCl) in water with a concentration of 2000 mg/L. The salt solute
165 rejection (R) was obtained at steady-state by Eq (2).

$$166 \quad R = 1 - \frac{C_p}{(C_0 + C_f) / 2} \quad (2)$$

167 where C_p and C_0 represent the concentration of the solute in the permeate and that in the
168 feed, respectively, while C_f is the concentration of the solute in the final concentrated feed.
169 Electric conductivity measured by calibrated ultrameter II 6PFC conductivity meter (Myron L
170 Company) was used as a proxy for salt concentration. The presented rejection values for each
171 sample are the average of three different measurements collected over a 60 min period.

172 2.6 Anti-fouling properties

173 The normalized permeate flux in the fouling stage was calculated using Eq. (3) [54][59]:

174
$$\text{normalized flux} = \frac{J}{J_0} \quad (3)$$

175 where J is the permeate flux at any given time during the test, and J_0 is the initial permeate
 176 flux. The slope of the plot of J/J_0 versus recovery rate (% , v/v) yielded the fouling propensity
 177 of the NF membranes [54].

178 To determine the surface tension characteristics of a solid surface, two of the three probe
 179 liquids should be polar and the other should be non-polar, and the test reagents must have
 180 high surface tension parameters [55]. In this study, the surface of the pristine NF membranes
 181 and the modified NF membranes are regarded as solid. The two polar liquids were ultrapure
 182 water and glycerol, while the non-polar liquid was diiodomethane. The surface tension
 183 properties of each probe liquid are listed in **Table S1 (SI)**. The surface tension parameters of
 184 the materials were calculated by measuring the direct contact angle of the three probe liquids
 185 and using a modified form of the extended Young equation given by:

186
$$\gamma_L^{\text{TOT}} = \gamma_L^{\text{LW}} + \gamma_L^{\text{AB}} \quad (4)$$

187
$$\gamma_L^{\text{AB}} = 2\sqrt{\gamma_L^+ \gamma_L^-} \quad (5)$$

188
$$(1 + \cos\theta)\gamma_L = 2(\sqrt{\gamma_S^{\text{LW}} \gamma_L^{\text{LW}}} + \sqrt{\gamma_S^+ \gamma_L^-} + \sqrt{\gamma_S^- \gamma_L^+}) \quad (6)$$

189 According to the ‘extended DLVO’ or ‘XDLVO’ theory, in the water environment, the
 190 interfacial energy between membranes and foulants is the sum of the Lifshitz–van der Waals
 191 (LW), electrostatic double layer (EL), and Lewis acid–base (AB) interactions. The
 192 electrostatic force (EL) interaction energy ($\Delta G_{\text{mlf}}^{\text{EL}}$) is also one component of the total
 193 interaction free energy, but it is much smaller than $\Delta G_{\text{mlf}}^{\text{TOT}}$, and can thus be neglected,
 194 resulting in:

195
$$\Delta G_{\text{mlf}}^{\text{TOT}} = \Delta G_{\text{mlf}}^{\text{LW}} + \Delta G_{\text{mlf}}^{\text{AB}} \quad (7)$$

$$\Delta G_{\text{mlf}}^{\text{LW}} = -2(\sqrt{\gamma_{\text{f}}^{\text{LW}}} - \sqrt{\gamma_{\text{l}}^{\text{LW}}})(\sqrt{\gamma_{\text{m}}^{\text{LW}}} - \sqrt{\gamma_{\text{l}}^{\text{LW}}}) \quad (8)$$

$$\Delta G_{\text{mlf}}^{\text{AB}} = 2[\sqrt{\gamma_{\text{l}}^+}(\sqrt{\gamma_{\text{m}}^-} + \sqrt{\gamma_{\text{f}}^-} - \sqrt{\gamma_{\text{l}}^-}) + \sqrt{\gamma_{\text{l}}^-}(\sqrt{\gamma_{\text{m}}^+} + \sqrt{\gamma_{\text{f}}^+} - \sqrt{\gamma_{\text{l}}^+}) - (\sqrt{\gamma_{\text{m}}^+ \gamma_{\text{f}}^-} + \sqrt{\gamma_{\text{m}}^- \gamma_{\text{f}}^+})] \quad (9)$$

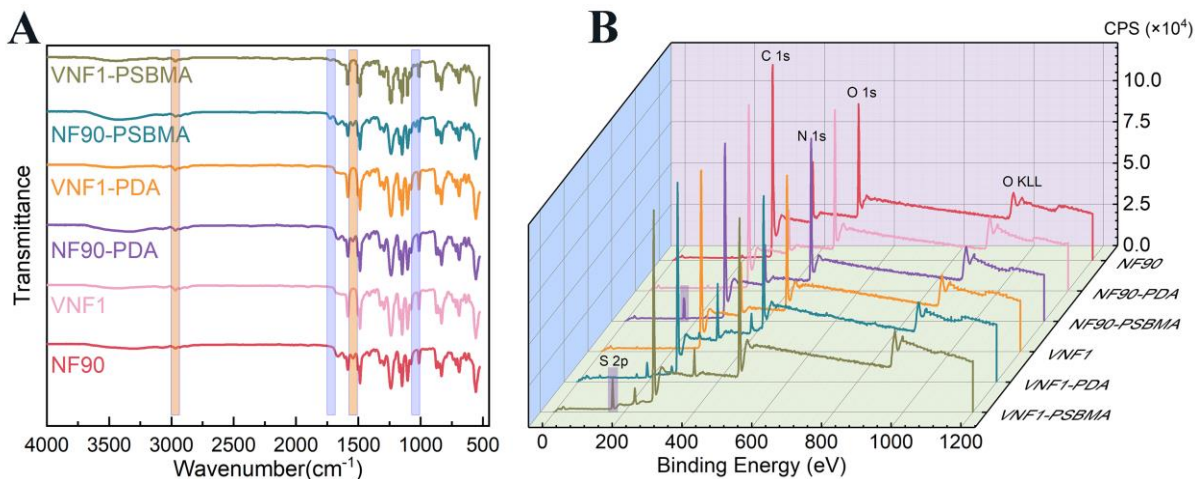
198 The subscripts f, l, and m represent the foulant, the liquid medium, and the membrane
 199 surface, respectively. Statistical analysis was performed with the statistical software SPSS
 200 18.0.

201 3. Results and discussion

202 3.1 Membrane surface properties

203 Membrane surface characteristics, such as chemical structure, hydrophilicity, roughness,
 204 and charge determine the separation performance and the anti-fouling properties of the
 205 membrane [42, 56]. **Fig. 1(A)** presents that the ATR-FTIR spectra determined between 500
 206 cm^{-1} and 4000 cm^{-1} for the pristine NF90 and VNF1 membranes, the BiBB-initiation-PDA
 207 mobilized membranes (NF90-PDA, VNF1-PDA), and the PDA-g-PSBMA modified NF
 208 membranes (NF90-PSBMA, VNF1-PSBMA). The stretching vibration peak at 1578, 1504,
 209 1487 cm^{-1} is attributed to the superposition of the peak of the polyamide layer and the
 210 polysulfone layer in the benzene ring plane. The characteristic peaks of the polysulfone
 211 support layer can be observed: specifically, the symmetric stretching vibration peaks of
 212 $\text{O}=\text{S}=\text{O}$ at 1167 and 1149 cm^{-1} , and the asymmetric stretching vibration peaks of $\text{O}=\text{S}=\text{O}$ at
 213 1320 and 1296 cm^{-1} . VNF1 series membranes are significantly different from NF90 series
 214 membranes in that only the latter showed peaks at 1610 cm^{-1} (H-bonded $\text{C}=\text{O}$ stretching) and
 215 1540 cm^{-1} (N–H in-plane bending and C–N bending vibration stretching vibration of the
 216 group $-\text{CO}-\text{NH}-$, amide II band) [57, 58]. Therefore, the characteristic peaks of amide II and
 217 arylamide were not observed for the VNF1 series membranes, suggesting that the latter
 218 consist of piperazine amide. The common peak between the two membranes at 1664 cm^{-1} is
 219 attributed to the amide I band ($\text{C}=\text{O}$ and C–N stretching vibration, C–C–N deformation
 220 vibration) [59, 60]. After the grafting of the PSBMA brushes, new peaks at 1715 and 1038

221 cm^{-1} emerged, attributed to ester and sulfonate groups of SBMA, respectively. These results
 222 preliminarily indicate that PSBMA was successfully grafted on the NF membrane surfaces
 223 [48, 61].



224
 225 **Fig. 1.** (A) ATR-FTIR spectra and (B) XPS spectra of pristine NF90 and VNF1 membranes
 226 and modified membranes prepared from PDA immobilization and PSBMA grafting.

227
 228 To further analyze the chemical composition of the NF90/VNF1 membrane surfaces
 229 before and after modification, XPS analysis was conducted and the resulting surface
 230 elemental compositions and spectra are presented in **Table 1** and **Fig. 1(B)**, respectively. An
 231 obvious increase in the O atom content and a decrease in N atom content were clearly
 232 observed upon PSBMA grafting. Consequently, the O/C atomic ratios of NF90-PSBMA and
 233 VNF1-PSBMA were respectively higher than those of NF90 and VNF1, while the N/C atomic
 234 ratios were lower. This result is rationalized with the fact that the grafted PSBMA has high
 235 O/C atomic ratio and low O/N atomic ratio compared with the pure polyamide. These results
 236 further confirm that PSBMA was successfully introduced onto the NF membrane surfaces.

237
 238 **Table 1** Surface elemental composition of the membranes.

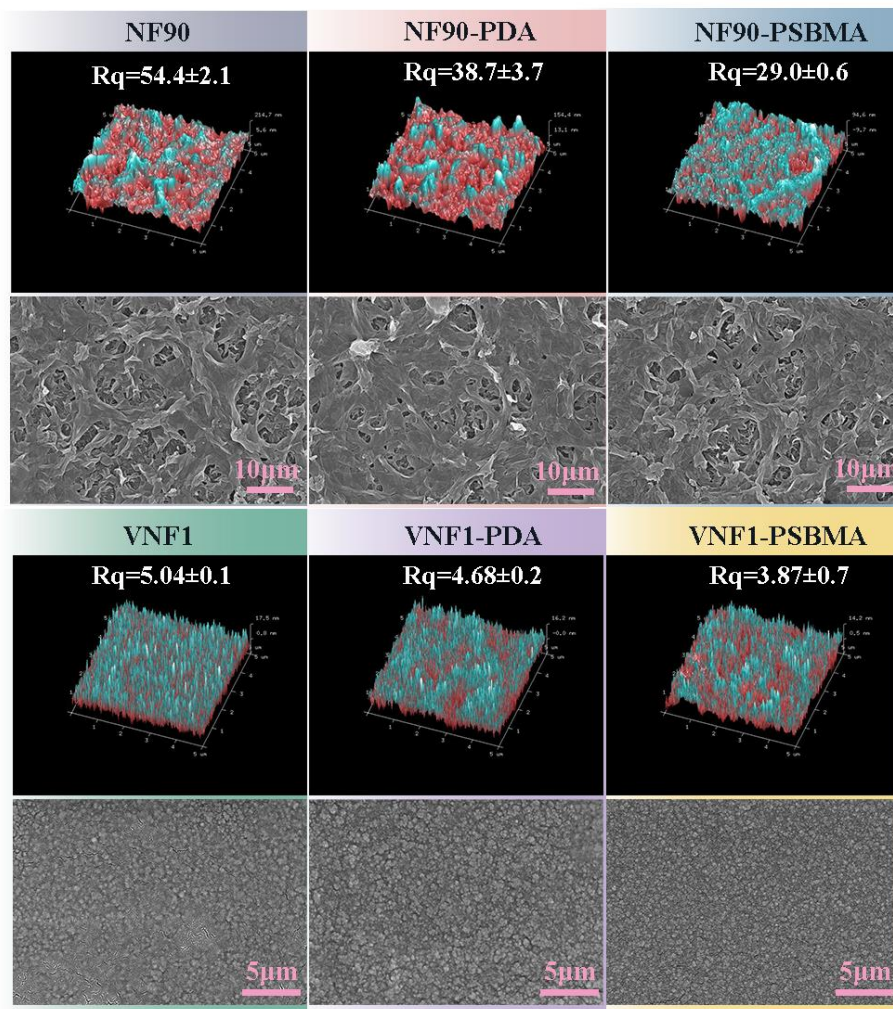
Membrane No.	Atomic percent (%)	Atomic ratio
--------------	--------------------	--------------

	C	N	O	Br	O/N	O/C
NF90	74.29	10.56	15.15	0	1.43	0.20
NF90-PDA	72.86	7.63	19.47	0.04	2.55	0.27
NF90-PSBMA	72.33	7.33	20.31	0.03	2.77	0.28
VNF1	74.52	8.54	16.81	0	1.97	0.23
VNF1-PDA	75.04	8.14	16.76	0.13	2.06	0.22
VNF1-PDA	73.64	4.62	21.67	0.07	4.69	0.29

239

240 3.2. Morphology analysis and surface charge

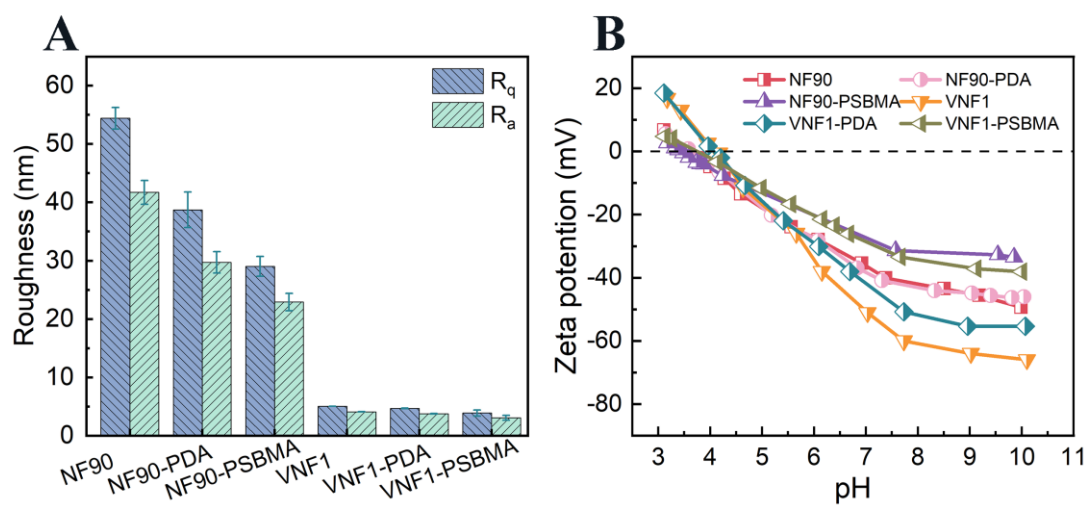
241 The morphology and roughness of the membrane surface influence the membrane
242 hydrophilicity, water flux, and the interactions between the surface and foulants. The surface
243 morphology of the NF90 and VNF1 membranes did not change significantly upon
244 modification with PSBMA (**Fig. 2**). According to the AFM results, the root means square
245 roughness parameters (R_q) of the NF90, NF90-PDA, and NF90-PSBMA membrane were
246 54.4 ± 2.1 nm, 38.7 ± 3.7 nm, and 29.0 ± 0.6 nm, respectively, while those of VNF1, VNF1-PDA,
247 and VNF1-PSBMA membrane were 5.04 ± 0.1 nm, 4.68 ± 0.2 nm, and 3.87 ± 0.7 nm,
248 respectively. Therefore, the roughness of the membrane surfaces decreased by approximately
249 20% after coating with PDA and by approximately 45% upon modification with the
250 zwitterion, with respect to the pristine membranes (**Fig. 3A**). This result suggest that the
251 modification steps may level out the surface features of polyamide. However, the initial
252 roughness of the two membranes was already small and the observed reduction was not
253 substantial in absolute terms, thus likely not resulting in significant changes in membrane
254 performance during operation.



255

256 **Fig. 2.** AFM and SEM images of pristine NF90 and VNF1 membranes and modified
 257 membranes prepared by immobilizing PDA and by grafting PSBMA.

258



259

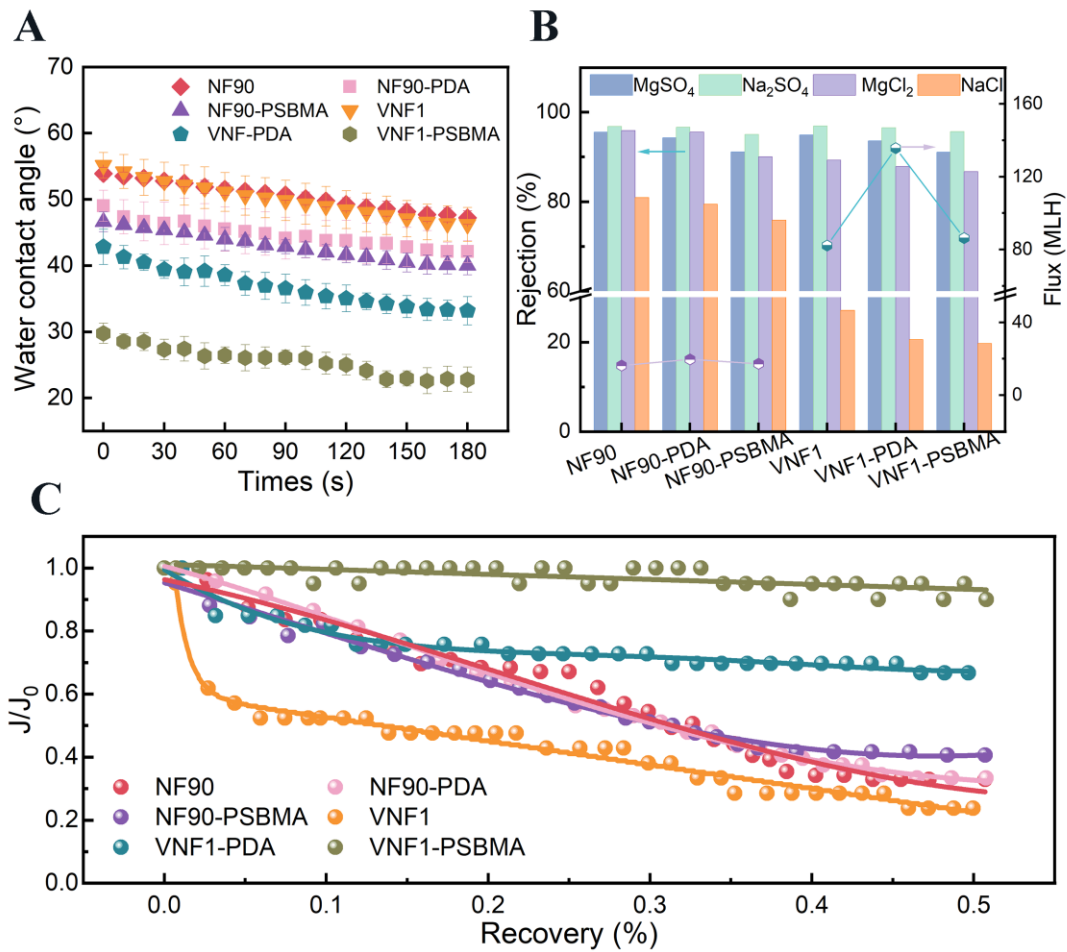
260 **Fig. 3. (A)** The average values of root mean-square (Rq) and average roughness (Ra) were
261 calculated from AFM images using at least six different locations on each membrane sample
262 (NF90, NF90-PDA, NF90-PSBMA, VNF1, VNF1-PDA and VNF1-PSBMA); **(B)** Surface
263 zeta potential values of pristine NF90 and VNF1 membrane and modified membranes as a
264 function of pH.

265

266 The surface properties of the modified membranes were further investigated by acquiring
267 zeta potential values. As shown in **Fig. 3B**, the pristine NF90 and VNF1 membranes had
268 highly negative electric potential, due to the carboxyl groups typically resulting from
269 interfacial polymerization of polyamide. With the coating of PDA, the amine and hydroxyl
270 groups of dopamine generally reduced the magnitude of the negative potential, which was
271 then further reduced upon SBMA grafting due to the net zero charge properties of the
272 zwitterions [62]. This trend was more pronounced in the VNF1 membrane samples, for which
273 a potential of larger magnitude was measured at the surface of the pristine membrane.
274 However, the zeta potential curves of the membranes modified with the PSBMA brush layer
275 was practically the same, regardless of the starting material, suggesting that the modification
276 was successful in both cases.

277 The wettability of the membrane surface was evaluated through water contact angle
278 measurements (**Fig. 4A**). The initial contact angles of pristine NF90 membrane, NF90-PDA
279 membrane, and NF90-PSBMA membrane were $55.2 \pm 0.9^\circ$, $48.7 \pm 1.5^\circ$, and $46.0 \pm 2.3^\circ$,
280 respectively, while the initial contact angles of pristine VNF1 membrane, VNF1-PDA
281 membrane, and VNF1-PSBMA membrane were $52.5 \pm 1.9^\circ$, $41.6 \pm 2.65^\circ$, and $28.4 \pm 0.99^\circ$,
282 respectively. The presence of PDA increased the wettability, although this enhancement effect
283 was minor, owing to the short reaction time (10 min). On the other hand, the water contact

284 angle decreased significantly after growth of the zwitterionic polymers brush, especially for
 285 the VNF1 samples.



286
 287 **Fig. 4.** (A) Water contact angle variation in time of pristine NF90 and VNF1 membranes and
 288 modified membranes; (B) Salt rejection values of pristine NF90 and VNF1 membrane and
 289 modified membranes (2.068 MPa, 25 °C, salt concentration: 2000 mg/L); (C) Permeate flux
 290 as a function of recovery rate for the different membranes (operating pressure: 2.068MPa;
 291 maximum water recovery: 50%).

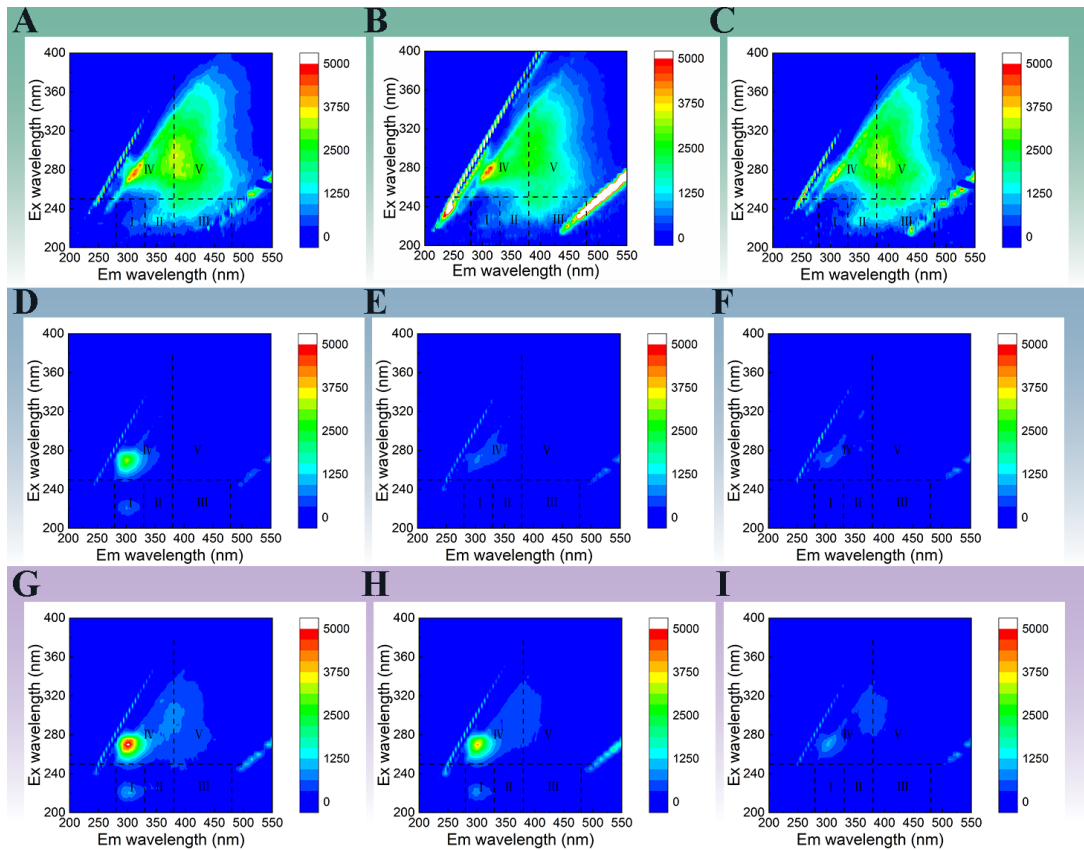
292
 293 Considering the selectivity shown in **Fig. 4B**, all the membranes had much higher rejection
 294 to divalent ions than monovalent ions, exhibiting a typical NF performance. In general, the
 295 observed rejection was in the order Na₂SO₄ > MgSO₄ > MgCl₂ > NaCl. With the coating of
 296 dopamine and the grafting of PSBMA, the retention rate of all the ions was slightly reduced,

297 but overall, there was no significant loss of the original retention rate. During filtration of
298 ultrapure water, the average flux were 16.2, 19.7, and 17.3 LMH for NF90, NF90-PDA and
299 NF90-PSBMA, while the permeate flux of VNF1-based samples were much higher, with
300 average fluxes equal to 82.2, 135.6, and 86.3 LMH for VNF1, VNF1-PDA and VNF1-
301 PSBMA, respectively. Compared to the VNF1 membranes, the NF90 membranes are denser
302 and therefore provide higher retention of monovalent ions and correspondingly lower fluxes.
303 In both cases, the flux increased significantly following PDA coating and returned to lower
304 values upon zwitterion brush formation. Ultimately, the values observed for the zwitterion-
305 grafted membranes were slightly higher than those measured for pristine membranes.

306 **Fig. 4C** illustrates the fouling behavior (revealing itself as a decrease in permeate flux [63])
307 of the membranes during the dead-end NF process for feed streams coinciding with the
308 effluents of integrated coagulation-UF pre-treatment. Grafting of SBMA greatly improved the
309 resistance to foulant deposition and to flux reduction. While the water flux was reduced
310 compared to the membranes with only PDA attached, the performance of the membranes
311 modified with PSBMA brushes was maintained for a longer period of time. The effect of
312 VNF1 modification was significantly better than that of NF90, consistent with the results of
313 FTIR and previous literature reports [13], likely due to the different chemistry of the
314 polyamide constituting the two membranes. The flux measured by deploying the VNF1-
315 PSBMA membrane was nearly constant during the filtration test, indicating negligible or
316 inconsequential deposition of foulants on these samples.

317 It is usually difficult to draw an overall profile of organic pollutants in shale gas
318 wastewaters and their process variations. Three-dimensional excitation-emission matrix
319 (EEM) fluorescence spectroscopy was used to analyze fluorescent organics compositions in a
320 complicated system such as the SWG of this study, by simultaneously varying the excitation
321 and emission wavelengths in real time (**Fig. 5**) [64]. As detailed in our previous study [29],

322 the fluorescence regional integration (FRI) method allowed classification of the organic
323 compounds in five domains: region I (Ex/Em = 220–250/280–330 nm, aromatic protein),
324 region II (Ex/Em = 220–250/330–380 nm, aromatic protein), region III (Ex/Em = 220–
325 250/380–480 nm, fulvic acid-like matters), region IV (Ex/Em = 250–440/280–380 nm,
326 soluble microbial by-product-like matters), and region V (Ex/Em = 250–400/380–540 nm,
327 humic acid-like components). According to the FRI under the EEM corresponding to each
328 region volume, almost no removal of dissolved organic matter was achieved after coagulation,
329 while the hybrid UF process mainly remove fulvic acid-like components, humic acid-like
330 components, and phenolic compounds (**Fig 6B**). The fraction of dissolved organics removed
331 by NF90 membrane was 94.1% for region III, 93.5% for region V, 87.7% for region II, 74.6%
332 for region IV, and 37.9% for region I. Larger removal rates were observed for the modified
333 NF90-PSBMA membranes, but in the same order: III (96.3%), V (95.4%), II (91.2%), IV
334 (88.7%), I (83.7%). The same order of removal rate was also determined for VNF1 samples,
335 with a higher rate relative to the modified membrane with respect to the pristine one.
336 Specifically, while the removal rate of dissolved organics by VNF1 was III (85.8%), V
337 (84.2%), II (78.6%), IV (51.1%), I (8.2%), that provided by VNF1-PSBMA was III (93.7%),
338 V (91.7%), II (90.5%), IV (85.5%), I (80.3%). These results and those presented in **Fig. 5**
339 clearly shows that the modified membranes improved the removal rate of organic matter in
340 each of the areas, but more markedly that of protein-like organic matter, which may be due to
341 the combination of increased membrane density and hydrophilicity following the surface
342 modification.



343

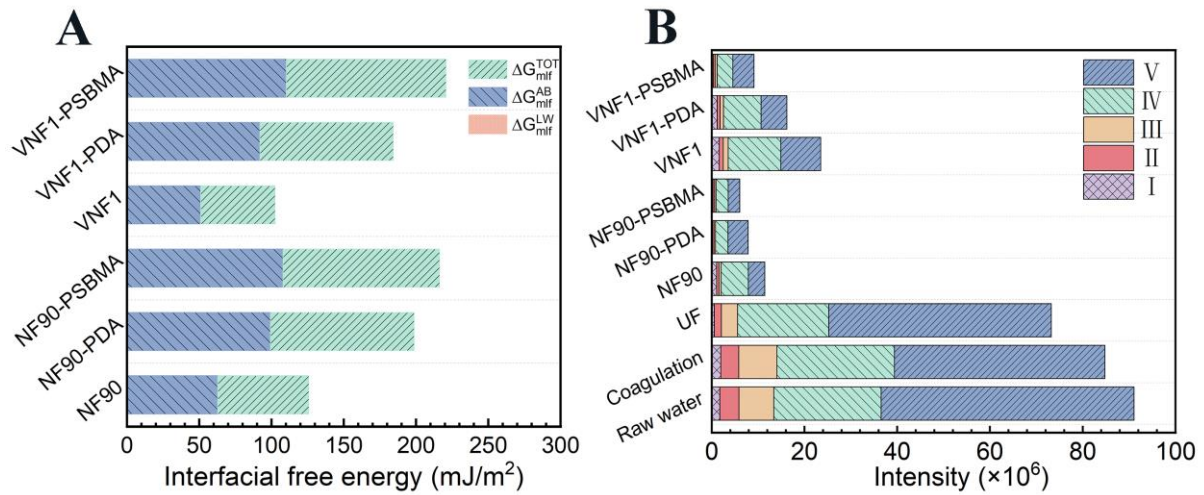
344 **Fig. 5.** Fluorescence excitation-emission matrix (EEM) of effluent water from each treatment
 345 process: (A) Raw water; (B) Coagulation; (C) Ultrafiltration; filtration through (D) NF90, (E)
 346 NF90-PDA, (F) NF90-PSBMA (G) VNF1, (H) VNF1-PDA, or (I) VNF1-PSBMA
 347 membranes. (I: tyrosine protein-like substances, II: tryptophan protein-like substances, III:
 348 fulvic-like substances, IV: soluble microbial byproducts, V: humic-like substances.)

349

350 3.4. Membrane-foulant physicochemical interactions

351 Extended XDLVO calculations are an accepted method to account for the interfacial
 352 forces between two surfaces at the microscopic scale [65]. In this paper, this theory was
 353 applied to investigate the main forces acting between the NF membranes and the SGW
 354 colloids. The contact angles of water, glycerol, and diiodomethane on the membrane surface
 355 and when in contact with a layer of SGW colloids are summarized in **Table S2 (SI)**. The
 356 resulting surface energy components (γ^{LW} , γ^+ , γ^-) were calculated using **eqs. 4-6**, and the

357 results are shown in **Table 2**. $\Delta G_{\text{mlf}}^{\text{LW}}$ and $\Delta G_{\text{mlf}}^{\text{AB}}$ were thus obtained with **eqs. 8** and **9**,
358 respectively, and the results are also presented in **Table 2**. Following surface grafting of the
359 zwitterionic polymers SBMA, the electron acceptor component (γ^+) slightly increased, while
360 the electron donor component (γ^-) increased importantly. This phenomenon is rationalized
361 mainly with the fact that the $-\text{SO}_3^-$ group of SBMA is negatively charged in water, and can
362 enhance the electron donating capability, hence the hydrophilicity of the membrane surface
363 [52]. Repulsion forces thwart the adsorption of contaminants on the membrane surface: the
364 more positive is the interaction energy, the more it is repulsive, and the membrane surface is
365 less likely to be fouled [66, 67]. Both AB and LW components of the membranes-SGW
366 colloids interaction had positive sign, thus the total interaction free energy ($\Delta G_{\text{mlf}}^{\text{TOT}}$) had
367 positive sign for all the membrane samples. Significantly, the surface grafting of SBMA
368 provided much more positive values of the total interfacial free energy, implying that the
369 zwitterionic SBMA brushes effectively reduced the likelihood of foulant adhesion on the
370 membrane surfaces. Furthermore, we found that the Lewis acid-base interaction energy
371 ($\Delta G_{\text{mlf}}^{\text{AB}}$) was much higher than the Lifshitzvan der Waals interaction energy ($\Delta G_{\text{mlf}}^{\text{LW}}$) and that
372 $\Delta G_{\text{mlf}}^{\text{LW}}$ remained almost unchanged after surface grafting, while $\Delta G_{\text{mlf}}^{\text{AB}}$ increased significantly.
373 Therefore, the Lewis acid-base interaction energy ($\Delta G_{\text{mlf}}^{\text{AB}}$) played the key role in controlling
374 membrane fouling.



375

376 **Fig. 6. (A)** Total interaction energy (ΔG_{mif}^{TOT}), Lifshitz–van der Waals interaction energy
 377 (ΔG_{mif}^{LW}), and Lewis acid–base (AB) interaction energy (ΔG_{mif}^{AB}) between the membranes and
 378 the SGW particles in aqueous solution; **(B)** Fluorescence region integral (FRI) results for
 379 samples from the effluent of each treatment process.

380

381 **Table 2**

382 The surface tension parameters and interfacial free energy of all membranes and SGW
 383 particles (mJ/m²).

Item	Surface tension parameter (mJ/m ²)					Free Energy		
	γ_L^{LW}	γ_L^-	γ_L^+	γ_L^{AB}	γ_L^{TOT}	ΔG^{LW}	ΔG^{AB}	ΔG^{TOT}
NF90	33.956	21.135	0.156	3.626	37.582	0.516	62.341	62.857
NF90-PDA	33.388	42.664	0.004	0.797	34.185	0.494	98.839	99.333
NF90- PSBMA	30.249	49.483	0.002	0.568	30.818	0.370	107.746	108.116
VNF1	33.608	20.041	2.224	13.354	46.961	0.502	50.695	51.198
VNF1-PDA	33.759	37.450	0.005	0.899	34.659	0.508	91.573	92.081
VNF1-	30.456	53.440	0.113	4.921	35.377	0.378	109.957	110.336

384

385 Conclusion

386 Zwitterionic SBMA brushes were grafted onto the surface of commercial NF membranes,
387 greatly improving the membrane antifouling ability and organic removal while retaining high
388 values of water permeability and only slightly decreasing the rejection rate of conventional
389 monovalent and divalent ions. The VNF1-PSBMA membrane exhibited very high
390 performance with pure water flux of 86.3 LMH, sodium sulfate removal rate of 95.67%, and
391 with the J/J_0 ratio upon fouling 73.54% higher than that related to the pristine VNF1
392 membrane at 50% recovery of SGW. All the dissolved organics were removed effectively by
393 the VNF1-PSBMA membrane, but especially the protein-like organic matter, which was not
394 rejected effectively by the pristine membranes. Antifouling and organic removal experiments
395 showed that the modification of membranes with grafted zwitterionic has high potential to
396 control membrane fouling and improve membrane performance in SGW reuse. This work
397 proposes a membrane modification that effectively affords better membrane performance,
398 particularly for the treatment of a highly complex wastewater from the shale gas industry,
399 thus providing a successful exploration of modified membrane materials and industrial
400 applications.

401

402 Acknowledgments

403 This work was supported by the National Natural Science Foundation of China
404 (52070134, 51678377), Xinglin Environment Project (2020CDYB-H02), and Sichuan
405 University and Yibin City People's Government strategic cooperation project (2019CDYB-
406 25). We would like to thank the Institute of New Energy and Low-Carbon Technology,

407 Sichuan University, for SEM measurement and the Analytical & Testing Center of Sichuan
408 University for XPS work and we would be grateful to Suilin Liu for his help of XPS analysis.

- 410 [1] C. Jia, M. Zheng, Y. Zhang, Unconventional hydrocarbon resources in China and the
411 prospect of exploration and development, *Petroleum Exploration and Development*, 39 (2012)
412 139-146.
- 413 [2] H. Chang, T. Li, B. Liu, R.D. Vidic, M. Elimelech, J.C. Crittenden, Potential and
414 implemented membrane-based technologies for the treatment and reuse of flowback and
415 produced water from shale gas and oil plays: A review, *Desalination*, 455 (2019) 34-57.
- 416 [3] C.L. Weber, C. Clavin, Life Cycle Carbon Footprint of Shale Gas: Review of Evidence
417 and Implications, *Environ. Sci. Technol.*, 46 (2012) 5688-5695.
- 418 [4] S. Jiang, J. Zhang, Z. Jiang, Z. Xu, D. Cai, L. Chen, Y. Wu, D. Zhou, Z. Jiang, X. Zhao, S.
419 Bao, Geology, resource potentials, and properties of emerging and potential China shale gas
420 and shale oil plays, *Interpretation*, 3 (2015) SJ1-SJ13.
- 421 [5] C.T. Montgomery, M.B. Smith, Hydraulic fracturing: History of an enduring technology,
422 *JPT, Journal of Petroleum Technology*, 62 (2010) 26-32.
- 423 [6] R. Beckwith, Hydraulic fracturing: The fuss, the facts, the future, *JPT, Journal of*
424 *Petroleum Technology*, 62 (2010) 34-41.
- 425 [7] Jackson, B. Robert, Vengosh, Avner, Davies, J. Richard, Carey, J. William, O'Sullivan,
426 Francis, The Environmental Costs and Benefits of Fracking, *Annual review of environment*
427 *and resources*, (2014).
- 428 [8] A. Kondash, A. Vengosh, Water Footprint of Hydraulic Fracturing, *Environmental*
429 *Science & Technology Letters*, 2 (2015) 276-280.
- 430 [9] N.A. Ahmad, P.S. Goh, L.T. Yogarathinam, A.K. Zulhairun, A.F. Ismail, Current
431 advances in membrane technologies for produced water desalination, *Desalination*, 493
432 (2020).
- 433 [10] B.C. Gordalla, U. Ewers, F.H. Frimmel, Hydraulic fracturing: a toxicological threat for
434 groundwater and drinking-water?, *Environmental Earth Sciences*, 70 (2013) 3875-3893.
- 435 [11] W. Shang, A. Tiraferri, Q. He, N. Li, H. Chang, C. Liu, B. Liu, Reuse of shale gas
436 flowback and produced water: Effects of coagulation and adsorption on ultrafiltration, reverse
437 osmosis combined process, *Sci. Total Environ.*, 689 (2019) 47-56.
- 438 [12] P. Tang, J. Li, T. Li, L. Tian, Y. Sun, W. Xie, Q. He, H. Chang, A. Tiraferri, B. Liu,
439 Efficient integrated module of gravity driven membrane filtration, solar aeration and GAC
440 adsorption for pretreatment of shale gas wastewater, *J. Hazard. Mater.*, (2020).
- 441 [13] H. Chang, B. Liu, B. Yang, X. Yang, C. Guo, Q. He, S. Liang, S. Chen, P. Yang, An
442 integrated coagulation-ultrafiltration-nanofiltration process for internal reuse of shale gas
443 flowback and produced water, *Sep. Purif. Technol.*, 211 (2019) 310-321.
- 444 [14] K.B. Gregory, R.D. Vidic, D.A. Dzombak, Water Management Challenges Associated
445 with the Production of Shale Gas by Hydraulic Fracturing, *Elements*, 7 (2011) 181-186.
- 446 [15] T. Tong, K.H. Carlson, C.A. Robbins, Z. Zhang, X. Du, Membrane-based treatment of
447 shale oil and gas wastewater: The current state of knowledge, *Frontiers of Environmental*
448 *Science and Engineering*, 13 (2019).
- 449 [16] B. Wang, M. Xiong, P. Wang, B. Shi, Chemical characterization in hydraulic fracturing
450 flowback and produced water (HF-FPW) of shale gas in Sichuan of China, *Environmental*
451 *Science and Pollution Research*, 27 (2020) 26532-26542.
- 452 [17] F.X. Kong, Z.P. Wang, Z. Ji, J.F. Chen, C.M. Guo, G.D. Sun, Y.F. Xie, Organic fouling
453 of membrane distillation for shale gas fracturing flowback water desalination: A special
454 interest in the feed properties by pretreatment, *Environmental Science: Water Research and*
455 *Technology*, 5 (2019) 1339-1348.

456 [18] D. Liu, J. Li, C. Zou, H. Cui, Y. Ni, J. Liu, W. Wu, L. Zhang, R. Coyte, A. Kondash, A.
457 Vengosh, Recycling flowback water for hydraulic fracturing in Sichuan Basin, China:
458 Implications for gas production, water footprint, and water quality of regenerated flowback
459 water, *Fuel*, 272 (2020) 117621.

460 [19] A.W. Mohammad, Y.H. Teow, W.L. Ang, Y.T. Chung, D.L. Oatley-Radcliffe, N. Hilal,
461 Nanofiltration membranes review: Recent advances and future prospects, *Desalination*, 356
462 (2015) 226-254.

463 [20] D. Zhou, L. Zhu, Y. Fu, M. Zhu, L. Xue, Development of lower cost seawater
464 desalination processes using nanofiltration technologies — A review, *Desalination*, 376
465 (2015) 109-116.

466 [21] D. Rana, T. Matsuura, Surface Modifications for Antifouling Membranes, *Chem. Rev.*,
467 110 (2010) 2448-2471.

468 [22] X. Zhao, R. Zhang, Y. Liu, M. He, Y. Su, C. Gao, Z. Jiang, Antifouling membrane
469 surface construction: Chemistry plays a critical role, *J. Membr. Sci.*, 551 (2018) 145-171.

470 [23] S. Jiang, Y. Li, B.P. Ladewig, A review of reverse osmosis membrane fouling and
471 control strategies, *Sci. Total Environ.*, 595 (2017) 567-583.

472 [24] T. Nguyen, F.A. Roddick, L. Fan, Biofouling of water treatment membranes: a review of
473 the underlying causes, monitoring techniques and control measures, *Membranes (Basel)*, 2
474 (2012) 804-840.

475 [25] E. Mohammad-Pajoo, D. Weichgrebe, G. Cuff, B.M. Tosarkani, K.-H. Rosenwinkel,
476 On-site treatment of flowback and produced water from shale gas hydraulic fracturing: A
477 review and economic evaluation, *Chemosphere*, 212 (2018) 898-914.

478 [26] W. Yu, T. Liu, J. Crawshaw, T. Liu, N. Graham, Ultrafiltration and nanofiltration
479 membrane fouling by natural organic matter: Mechanisms and mitigation by pre-ozonation
480 and pH, *Water Res.*, 139 (2018) 353-362.

481 [27] F.-x. Kong, J.-f. Chen, H.-m. Wang, X.-n. Liu, X.-m. Wang, X. Wen, C.-m. Chen, Y.F.
482 Xie, Application of coagulation-UF hybrid process for shale gas fracturing flowback water
483 recycling: Performance and fouling analysis, *J. Membr. Sci.*, 524 (2017) 460-469.

484 [28] Y. Liu, P. Tang, Y. Zhu, W. Xie, P. Yang, Z. Zhang, B. Liu, Green aerogel adsorbent for
485 removal of organic compounds in shale gas wastewater: High-performance tuning and
486 adsorption mechanism, *Chem. Eng. J.*, 416 (2021) 129100.

487 [29] P. Tang, B. Liu, Y. Zhang, H. Chang, P. Zhou, M. Feng, V.K. Sharma, Sustainable reuse
488 of shale gas wastewater by pre-ozonation with ultrafiltration-reverse osmosis, *Chem. Eng. J.*,
489 392 (2020) 123743.

490 [30] P. Tang, W. Xie, A. Tiraferri, Y. Zhang, J. Zhu, J. Li, D. Lin, J.C. Crittenden, B. Liu,
491 Organics removal from shale gas wastewater by pre-oxidation combined with biologically
492 active filtration, *Water Res.*, 196 (2021) 117041.

493 [31] Y.-C. Chiang, Y. Chang, C.-J. Chuang, R.-C. Ruaan, A facile zwitterionization in the
494 interfacial modification of low bio-fouling nanofiltration membranes, *J. Membr. Sci.*, 389
495 (2012) 76-82.

496 [32] T. Sun, Y. Liu, L. Shen, Y. Xu, R. Li, L. Huang, H. Lin, Magnetic field assisted
497 arrangement of photocatalytic TiO₂ particles on membrane surface to enhance membrane
498 antifouling performance for water treatment, *J. Colloid Interface Sci.*, 570 (2020) 273-285.

499 [33] M. He, K. Gao, L. Zhou, Z. Jiao, M. Wu, J. Cao, X. You, Z. Cai, Y. Su, Z. Jiang,
500 Zwitterionic materials for antifouling membrane surface construction, *Acta Biomater.*, 40
501 (2016) 142-152.

502 [34] Z. Wang, D. Hou, S. Lin, Composite Membrane with Underwater-Oleophobic Surface
503 for Anti-Oil-Fouling Membrane Distillation, *Environ. Sci. Technol.*, 50 (2016) 3866-3874.

504 [35] F.-x. Kong, G.-d. Sun, J.-f. Chen, J.-d. Han, C.-m. Guo, Z. Tong, X.-f. Lin, Y.F. Xie,
505 Desalination and fouling of NF/low pressure RO membrane for shale gas fracturing flowback
506 water treatment, *Sep. Purif. Technol.*, 195 (2018) 216-223.

507 [36] X. Chen, T. Taguchi, Enhanced Skin Adhesive Property of Hydrophobically Modified
508 Poly(vinyl alcohol) Films, *ACS Omega*, 5 (2020) 1519-1527.

509 [37] D.T. Auguste, R.K. Prud'homme, P.L. Ahl, P. Meers, J. Kohn, Polymer-Protected
510 Liposomes: Association of Hydrophobically-Modified PEG with Liposomes, in: *Polymeric*
511 *Drug Delivery I*, American Chemical Society, 2006, pp. 95-120.

512 [38] H. Huang, Y. Sun, L. Cui, Y. Ni, S. Li, W. Xing, W. Jing, Generation of Monodisperse
513 Submicron Water-in-Diesel Emulsions via a Hydrophobic MXene-Modified Ceramic
514 Membrane, *Ind. Eng. Chem. Res.*, 59 (2020) 20349-20358.

515 [39] C. Zhao, X. Yu, X. Da, M. Qiu, X. Chen, Y. Fan, Fabrication of a charged
516 PDA/PEI/Al₂O₃ composite nanofiltration membrane for desalination at high temperatures,
517 *Sep. Purif. Technol.*, 263 (2021) 118388.

518 [40] P. Kanagaraj, I.M.A. Mohamed, W. Huang, C. Liu, Membrane fouling mitigation for
519 enhanced water flux and high separation of humic acid and copper ion using hydrophilic
520 polyurethane modified cellulose acetate ultrafiltration membranes, *Reactive and Functional*
521 *Polymers*, 150 (2020) 104538.

522 [41] H. Liu, Z. Ma, W. Yang, X. Pei, F. Zhou, Facile preparation of structured zwitterionic
523 polymer substrate via sub-surface initiated atom transfer radical polymerization and its
524 synergistic marine antifouling investigation, *Eur. Polym. J.*, 112 (2019) 146-152.

525 [42] Q. Li, X. Zhang, H. Yu, H. Zhang, J. Wang, A facile surface modification strategy for
526 improving the separation, antifouling and antimicrobial performances of the reverse osmosis
527 membrane by hydrophilic and Schiff-base functionalizations, *Colloids and Surfaces A:*
528 *Physicochemical and Engineering Aspects*, 587 (2020) 124326.

529 [43] C. Liu, A.F. Faria, J. Ma, M. Elimelech, Mitigation of Biofilm Development on Thin-
530 Film Composite Membranes Functionalized with Zwitterionic Polymers and Silver
531 Nanoparticles, *Environ. Sci. Technol.*, 51 (2017) 182-191.

532 [44] M.S. Rahaman, H. Therien-Aubin, M. Ben-Sasson, C.K. Ober, M. Nielsen, M.
533 Elimelech, Control of biofouling on reverse osmosis polyamide membranes modified with
534 biocidal nanoparticles and antifouling polymer brushes, *J Mater Chem B*, 2 (2014) 1724-
535 1732.

536 [45] D. Saeki, T. Tanimoto, H. Matsuyama, Anti-biofouling of polyamide reverse osmosis
537 membranes using phosphorylcholine polymer grafted by surface-initiated atom transfer
538 radical polymerization, *Desalination*, 350 (2014) 21-27.

539 [46] J. Wang, Z. Wang, J. Wang, S. Wang, Improving the water flux and bio-fouling
540 resistance of reverse osmosis (RO) membrane through surface modification by zwitterionic
541 polymer, *J. Membr. Sci.*, 493 (2015) 188-199.

542 [47] G. Ye, J. Lee, F. Perreault, M. Elimelech, Controlled Architecture of Dual-Functional
543 Block Copolymer Brushes on Thin-Film Composite Membranes for Integrated “Defending”
544 and “Attacking” Strategies against Biofouling, *ACS Appl. Mater. Interfaces*, 7 (2015) 23069-
545 23079.

546 [48] W.-W. Yue, H.-J. Li, T. Xiang, H. Qin, S.-D. Sun, C.-S. Zhao, Grafting of zwitterion
547 from polysulfone membrane via surface-initiated ATRP with enhanced antifouling property
548 and biocompatibility, *J. Membr. Sci.*, 446 (2013) 79-91.

549 [49] H. Chang, T. Li, B. Liu, C. Chen, Q. He, J.C. Crittenden, Smart ultrafiltration membrane
550 fouling control as desalination pretreatment of shale gas fracturing wastewater: The effects of
551 backwash water, *Environ. Int.*, 130 (2019) 104869.

552 [50] K. Matyjaszewski, Atom Transfer Radical Polymerization (ATRP): Current status and
553 future perspectives, *Macromolecules*, 45 (2012) 4015-4039.

554 [51] K. Matyjaszewski, D. Hongchen, W. Jakubowski, J. Pietrasik, A. Kusumo, Grafting from
555 surfaces for "everyone": ARGET ATRP in the presence of air, *Langmuir*, 23 (2007) 4528-
556 4531.

557 [52] W. Xie, A. Tiraferri, X. Ji, C. Chen, Y. Bai, J.C. Crittenden, B. Liu, Green and
558 sustainable method of manufacturing anti-fouling zwitterionic polymers-modified poly(vinyl
559 chloride) ultrafiltration membranes, *J. Colloid Interface Sci.*, 591 (2021) 343-351.

560 [53] M. He, T. Li, M. Hu, C. Chen, B. Liu, J. Crittenden, L.-Y. Chu, H.Y. Ng, Performance
561 improvement for thin-film composite nanofiltration membranes prepared on PSf/PSf-g-PEG
562 blended substrates, *Sep. Purif. Technol.*, 230 (2020) 115855.

563 [54] S. Hong, M. Elimelech, Chemical and physical aspects of natural organic matter (NOM)
564 fouling of nanofiltration membranes, *J. Membr. Sci.*, 132 (1997) 159-181.

565 [55] W. Wu, R.F. Giese, C.J. van Oss, Stability versus flocculation of particle suspensions in
566 water—correlation with the extended DLVO approach for aqueous systems, compared with
567 classical DLVO theory, *Colloids and Surfaces B: Biointerfaces*, 14 (1999) 47-55.

568 [56] A. Tiraferri, Y. Kang, E.P. Giannelis, M. Elimelech, Highly Hydrophilic Thin-Film
569 Composite Forward Osmosis Membranes Functionalized with Surface-Tailored
570 Nanoparticles, *ACS Appl. Mater. Interfaces*, 4 (2012) 5044-5053.

571 [57] C.Y. Tang, Y.-N. Kwon, J.O. Leckie, Effect of membrane chemistry and coating layer on
572 physiochemical properties of thin film composite polyamide RO and NF membranes: II.
573 Membrane physiochemical properties and their dependence on polyamide and coating layers,
574 *Desalination*, 242 (2009) 168-182.

575 [58] A. Simon, W.E. Price, L.D. Nghiem, Influence of formulated chemical cleaning reagents
576 on the surface properties and separation efficiency of nanofiltration membranes, *J. Membr.*
577 *Sci.*, 432 (2013) 73-82.

578 [59] M.F. Jimenez Solomon, Y. Bhole, A.G. Livingston, High flux membranes for organic
579 solvent nanofiltration (OSN)—Interfacial polymerization with solvent activation, *J. Membr.*
580 *Sci.*, 423-424 (2012) 371-382.

581 [60] Y. Li, E. Wong, Z. Mai, B. Van der Bruggen, Fabrication of composite
582 polyamide/Kevlar aramid nanofiber nanofiltration membranes with high permselectivity in
583 water desalination, *J. Membr. Sci.*, 592 (2019).

584 [61] M.R. De Guzman, C.K.A. Andra, M.B.M.Y. Ang, G.V.C. Dizon, A.R. Caparanga, S.-H.
585 Huang, K.-R. Lee, Increased performance and antifouling of mixed-matrix membranes of
586 cellulose acetate with hydrophilic nanoparticles of polydopamine-sulfobetaine methacrylate
587 for oil-water separation, *J. Membr. Sci.*, 620 (2021) 118881.

588 [62] Q. Shi, Y. Su, W. Zhao, C. Li, Y. Hu, Z. Jiang, S. Zhu, Zwitterionic Polyethersulfone
589 Ultrafiltration Membrane with Superior Antifouling Property, *J. Membr. Sci.*, 319 (2008) 271.

590 [63] Z. He, D.J. Miller, S. Kasemset, D.R. Paul, B.D. Freeman, The effect of permeate flux on
591 membrane fouling during microfiltration of oily water, *J. Membr. Sci.*, 525 (2017) 25-34.

592 [64] J. Guo, X. Zhu, Q. Wang, W. Liu, Y. Wang, The combination effect of preozonation and
593 CNTs layer modification on low-pressure membrane fouling control in treating NOM and
594 EfOM, *J. Membr. Sci.*, 627 (2021) 119225.

595 [65] M. Zhang, X. Zhou, L. Shen, X. Cai, F. Wang, J. Chen, H. Lin, R. Li, X. Wu, B.-Q. Liao,
596 Quantitative evaluation of the interfacial interactions between a randomly rough sludge floc
597 and membrane surface in a membrane bioreactor based on fractal geometry, *Bioresour.*
598 *Technol.*, 234 (2017) 198-207.

599 [66] C. Liu, D. Song, W. Zhang, Q. He, X. Huangfu, S. Sun, Z. Sun, W. Cheng, J. Ma,
600 Constructing zwitterionic polymer brush layer to enhance gravity-driven membrane
601 performance by governing biofilm formation, *Water Res.*, 168 (2020) 115181.

602 [67] N. Subhi, A.R.D. Verliefde, V. Chen, P. Le-Clech, Assessment of physicochemical
603 interactions in hollow fibre ultrafiltration membrane by contact angle analysis, J. Membr.
604 Sci., 403-404 (2012) 32-40.

605 **Graphical abstract**

